CHEMISTRY OF MATERIALS

Article

pubs.acs.org/cm

Porous Hydroxide Nanosheets on Preformed Nanowires by Electrodeposition: Branched Nanoarrays for Electrochemical Energy Storage

Xinhui Xia,[†,‡] Jiangping Tu,[†,*] Yongqi Zhang,[†] Jiao Chen,[†] Xiuli Wang,[†] Changdong Gu,[†] Cao Guan,[‡] Jingshan Luo,[‡] and Hong Jin Fan[‡,*]

[†]State Key Laboratory of Silicon Materials and Department of Materials Science and Engineering, Zhejiang University, Hangzhou 310027, P. R. China

[‡]Division of Physics and Applied Physics, School of Physical and Mathematical Sciences, Nanyang Technological University, Singapore 637371, Singapore

Supporting Information

ABSTRACT: Fast, high-yield, and controllable synthesis of functional hydroxide and oxide nanomaterials on conductive substrates is highly desirable for the energy generation and storage applications. For the same purpose, three-dimensional hierarchical porous nanostructures are being regarded advantageous. In this work, we report the fabrication of porous metal hydroxide nanosheets on a preformed nanowires scaffold using the fast and well-controllable electrodeposition method. $Co(OH)_2$ and $Mn(OH)_2$ nanosheets are electrochemically deposited on the Co_3O_4 core nanowires to form core/shell arrays. Such oxide/hydroxide core/shell nanoarrays can be realized on various conductive substrates. The $Co_3O_4/Co(OH)_2$ core/shell nanowire arrays are evaluated as a supercapacitor cathode material that exhibits high specific capacitances of 1095 F/g at 1 A/g and 812 F/g at 40 A/g, respectively. The mesoporous homogeneous Co_3O_4 core/shell nanowire arrays, obtained by annealing the $Co_3O_4/Co(OH)_2$ sample, are applied as the anode material for lithium ion batteries. A high capacity of 1323 mAh/g at 0.5 C and excellent cycling stability are demonstrated. Our results show that electrodeposition is a versatile technique for fabrication of nanometal oxides on 3-D templates for electrochemical energy applications.

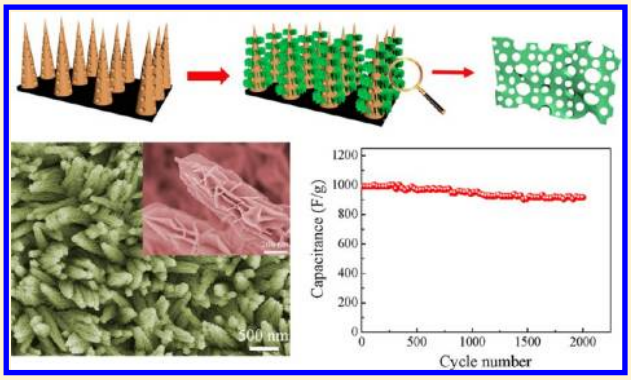

KEYWORDS: *core−shell, nanowires, metal oxides, porous film, supercapacitor, lithium ion battery*

INTRODUCTION

Freestanding one-dimensional (1D) core/shell nanowire arrays have sparked great interest due to their enhanced physical and chemical properties as compared to the single components.[1,2] Controllable synthesis of complex core/shell nanowire arrays with hierarchically porous structures is a prerequisite for the construction of high-performance electronic and electrochemical energy storage devices because they not only provide large active surface area and short diffusion path lengths to electrons and ions but also show a potential synergistic effect through modification by each other, leading to high charge/discharge rates and high energy conversion efficiency.[3−7] Great efforts have been devoted to the synthesis of self-supported core/shell nanowire arrays. Generally, two synthetic protocols have been put forward for the fabrication of self-supported core/shell nanowire arrays: (1) One-step synthesis method and (2) stepwise synthetic approach. For the first strategy, it always needs sacrificial templates such as AAO template to integrate the target materials via wet-chemical solution methods.[8] This one-step method is limited to simple geometry or flat surfaces and involves etching away the template, but this etching process will cause the collapse of the target core/shell nanowire arrays leading to misoriented structures. Besides, it is difficult to prepare core/shell nanowire arrays with hierarchically porous strucuture with the template method. To date, most of the core/shell nanowire arrays are prepared based on the second approach, which first constructs a freestanding nanowire core backbone and subsequently coats the shell materials. This method needs to combine different methods such as hydrothermal synthesis,[5] sputtering,[9,10] electrodeposition,[11,12] chemical bath deposition,[13] thermal oxidation,[14] and pulsed laser deposition[15] to prepare advanced core/shell nanowire arrays. Various types of core/shell nanowire arrays whose core or shell materials consist of metals, oxides, carbon, hydroxides, semiconductors, and polymers have been prepared via a stepwise synthetic approach.[1,2,7] Despite this progress, the

Received: July 31, 2012
Revised: September 17, 2012
Published: September 20, 2012

fabrication of self-supported metal oxide/hydroxide core/shell nanowire arrays with crystalline porous architectures still remains a significant challenge.

Transition metal oxides and hydroxides such as Co_3O_4, $Co(OH)_2$, Mn_3O_4, and $Mn(OH)_2$ are important materials for electrochemical energy storage, sensors, and catalysis.[16,17] Integration of these oxides and hydroxides into core/shell nanowire arrays with hierarchically porous structure may exhibit unprecedented physical and electrochemical properties due to the effects of spatial confinement and potential synergetic effect. Up to now, there are a few reports on transition metal oxide/hydroxide core/shell nanowire arrays. Previously, we developed two-step hydrothermal synthesis methods for the fabrication of CoO/$Ni(OH)_2$[18] and ZnO/$Ni(OH)_2$[19] core/shell nanowire arrays for supercapacitors. In the present work, we introduce another simple and general method to prepare porous hydroxide nanosheets on preformed nanowires to form core/shell branched nanoarrays including Co_3O_4/$Co(OH)_2$ and Co_3O_4/$Mn(OH)_2$ on various conductive substrates. This new synthetic strategy is based on the combination of hydrothermal synthesis and electrodeposition methods, which shows unique principles and flexibility in the control of the structure and morphology of target materials. By thermal annealing, the porous hydroxide nanosheets can be converted into the corresponding mesoporous metal oxides to form hierarchically porous metal oxide core/shell nanowire arrays. As a demonstration, we investigate the electrochemical properties of Co_3O_4/$Co(OH)_2$ core/shell nanowire arrays and homogeneous mesoporous Co_3O_4 core/shell nanowire arrays obtained by annealing the Co_3O_4/$Co(OH)_2$ sample for electrochemical energy storage. In this report, the Co_3O_4/$Co(OH)_2$ core/shell nanowire arrays grown on nickel foam are found to be promising pseudocapacitive materials with high capacitance and rather good rate capability. As the anode material for lithium ion batteries, the mesoporous Co_3O_4 core/shell nanowire arrays show superior electrochemical performance with excellent capacity retention and high-rate performance.

EXPERIMENTAL SECTION

All solvents and chemicals were of reagent quality and used without further purification. The cobalt nitrate, sodium nitrate, cobalt acetate, and ammonia (25−28%) were obtained from Shanghai Chemical Reagent Co. All aqueous solutions were freshly prepared with high purity water (18 MΩ cm resistance).

Preparation of Co_3O_4/$Co(OH)_2$ and Mesoporous Co_3O_4 Core/Shell Nanowire Arrays. First, self-supported Co_3O_4 nanowire arrays were prepared by a facile hydrothermal synthesis method according to our previous work.[13] The reaction solution was obtained by mixing 1.5 mmol of $Co(NO_3)_2$, 3 mmol of NH_4F, and 7.5 mmol of $CO(NH_2)_2$ in 50 mL of distilled water and then transferred into Teflon-lined stainless steel autoclave liners. Various substrates (2×6 cm^2 in sizes) such as nickel foam, stainless steel substrate, and Ti foil were immersed into the reaction solution. The nickel foam substrate was rolled to a thickness of 0.72 mm before use. The top sides of the substrates were uniformly coated with a polytetrafluoroethylene tape to prevent the solution contamination. The liner was sealed in a stainless steel autoclave and maintained at 110 °C for 5 h and then cooled down to room temperature. The samples were collected and rinsed with distilled water several times. Finally, the samples were annealed at 350 °C in normal purity argon for 2 h to obtain self-supported Co_3O_4 nanowire arrays. Then, the self-supported Co_3O_4 nanowire arrays were used as the scaffold for $Co(OH)_2$ nanosheet shell growth through a simple cathodic electrodeposition method. The electrodeposition was performed in a standard three-electrode glass cell at 25 °C, the above self-supported Co_3O_4 nanowire arrays electrode as the working electrode, saturated calomel electrode (SCE) as the reference electrode, and a Pt foil as the counter-electrode. The electrolyte for electrodeposition of $Co(OH)_2$ was obtained by dissolving 8.5 g of $Co(NO_3)_2$ into 100 mL of distilled water. The $Co(OH)_2$ shell nanosheet was deposited by cyclic voltammetry (CV) as follows: The CV deposition was conducted in the potential range of −0.5 to −1.1 V with a sweep rate of 10 mV/s for 4 cycles. The substrates were taken off and rinsed with distilled water. The samples were annealed at 200 °C in air for 1.5 h to form homogeneous mesoporous Co_3O_4 core/shell nanorod arrays. The Co_3O_4/$Mn(OH)_2$ and Co_3O_4/Mn_3O_4 nanowire arrays were fabricated under the same preparation parameters.

Characterization of Core/Shell Nanowire Arrays. The samples were characterized by X-ray diffraction (XRD, RIGAKU D/Max-2550 with Cu Kα radiation), field emission scanning electron microscopy (FESEM, FEI SIRION), and high-resolution transmission electron microscopy (HRTEM, JEOL JEM-2010F). The surface area of the film that was scratched from the substrate was determined by BET measurements using a NOVA-1000e surface area analyzer.

Electrochemical Measurements of Co_3O_4/$Co(OH)_2$ Nanowire Arrays. The electrochemical measurements of the Co_3O_4/$Co(OH)_2$ core/shell nanowire arrays were carried out in a three-electrode electrochemical cell containing 2 M KOH aqueous solution as the electrolyte. Cyclic voltammetry (CV) measurements were performed on a CHI660c electrochemical workstation (Chenhua, Shanghai). CV measurements were carried out at a scanning rate of 10 mV/s between −0.1 and 0.6 V at 25 °C. The nanowire arrays (≈2×3 cm^2, Co_3O_4 mass ≈ 1.2 mg/cm^2, $Co(OH)_2$ mass ≈ 0.3 mg cm^{-2}) were the working electrode, Hg/HgO was the reference electrode, and a Pt foil was used as the counter-electrode. The galvanostatic charge/discharge tests were conducted on a LAND battery program-control test system. The nanowire arrays electrode, together with a nickel mesh counter electrode and an Hg/HgO reference electrode, was tested in a three-compartment system. The specific capacitance is calculated according to the following equation: $C = I\Delta t/M\Delta V$, where C (F/g) was specific capacitance, I (mA) represented discharge current, and M (mg), ΔV (V), and Δt (s) designated mass of active materials, potential drop during discharge, and total discharge time, respectively.

Electrochemical Measurements of Mesoporous Co_3O_4 Nanowire Arrays. CR2025 coin-type cells were directly fabricated from the mesoporous Co_3O_4 nanowire arrays on nickel foam as the working electrode (Co_3O_4 mass ≈ 1.4 mg/cm^2) without any ancillary materials. A metallic lithium foil served as the counter electrode, 1 M $LiPF_6$ in ethylene carbonate (EC)−dimethyl carbonate (DMC) (1: 1 in volume) was used as the electrolyte, and a polypropylene microporous film (Cellgard 2300) was used as the separator. The cells were assembled in an argon-filled glovebox with high-purity argon gas (99.9995% purity). The galvanostatic charge−discharge tests were performed on a LAND battery program-control test system (Wuhan, China) between 0 and 3 V at room temperature. The cyclic voltammetry (CV) test was carried out on a CHI660C electrochemical workstation (Chenhua, Shanghai) in the potential window of 0−3 V (vs Li/Li^+) at a scan rate of 0.1 mV/s.

RESULTS AND DISCUSSION

Figure 1 depicts the formation process of branched nanowire arrays by electrodeposition on preformed nanowire arrays. The unidirectional nanowires can be metal oxides, sulfides, or even metals obtained through any solution or vapor-phase method on various conductive substrates (e.g., nickel foam, stainless steel, and Ti foil). We take Co_3O_4 nanowires by hydrothermal growth on nickel foam as an example. Metal hydroxide nanoflakes such as $Co(OH)_2$ and $Mn(OH)_2$ are cathodic electrodeposited directly on the Co_3O_4 nanowires to create the branched core/shell nanoarrays. It is noteworthy that these hydroxide nanoflakes are highly porous. They can be further converted to mesoporous oxides by thermal annealing. This

dx.doi.org/10.1021/cm302416d | Chem. Mater. 2012, 24, 3793−3799

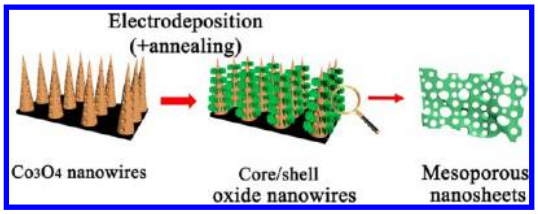

Figure 1. Schematics of porous hydroxide nanosheets formed by electrodeposition on preformed nanowire arrays. The hydroxide sheets can be converted into oxides by thermal annealing.

stepwise approach allows us to directly fabricate hierarchical nanostructures over large areas on substrates.

We choose the $Co_3O_4/Co(OH)_2$ core/shell nanowire arrays on nickel foam as an illustrative case. The obtained Co_3O_4 nanowires have diameters of ~70 nm and grow nearly vertical to the substrate forming nanowires arrays (Figure 2a,b and

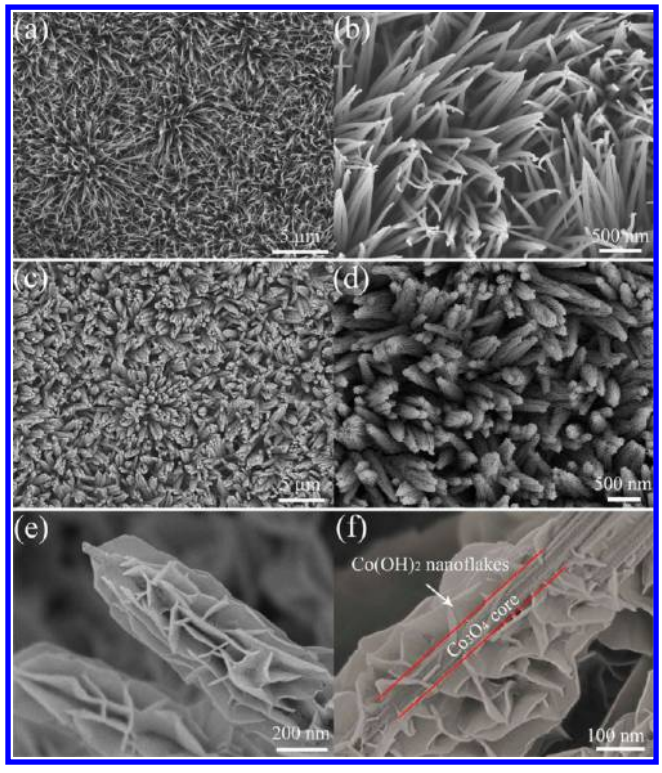

Figure 2. Electrodeposition of $Co(OH)_2$ nanosheet branches on Co_3O_4 nanowires. (a, b) SEM images of Co_3O_4 nanowire arrays on nickel foam. (c, d) $Co_3O_4/Co(OH)_2$ core/shell nanowire arrays. (e) Fine view and (f) profile image of a single core/shell nanowire.

Supporting Information Figure S1). After electrodeposition, the Co_3O_4 nanowires are uniformly covered by $Co(OH)_2$ nanosheets with an overall size of ~20 nm (Figure 2c,d). This core/shell heterostructure is further demonstrated by the magnified fine structure and profile section SEM images of the individual nanowire in Figure 2e,f. X-ray diffraction (XRD) patterns reveal the presence of the crystalline spinel Co_3O_4 (JCPDS 42-1467) and α-$Co(OH)_2$ (JCPDS 74-1057) (Supporting Information Figure S1c). The $Co_3O_4/Co(OH)_2$ core/shell nanowire arrays grown on other substrates (such as stainless steel and Ti foil) show similar morphologies as described above (Supporting Information Figure S2), indicating that the substrate geometry has no significant effect on the final morphology.

Further insight into the detailed microstructure of the core/shell nanowire is elucidated by TEM and HRTEM. The Co_3O_4 nanowires possess mesoporous walls ranging from 2−4 nm (Figure 3a,b). The measured lattice spacing of 0.46 nm is in

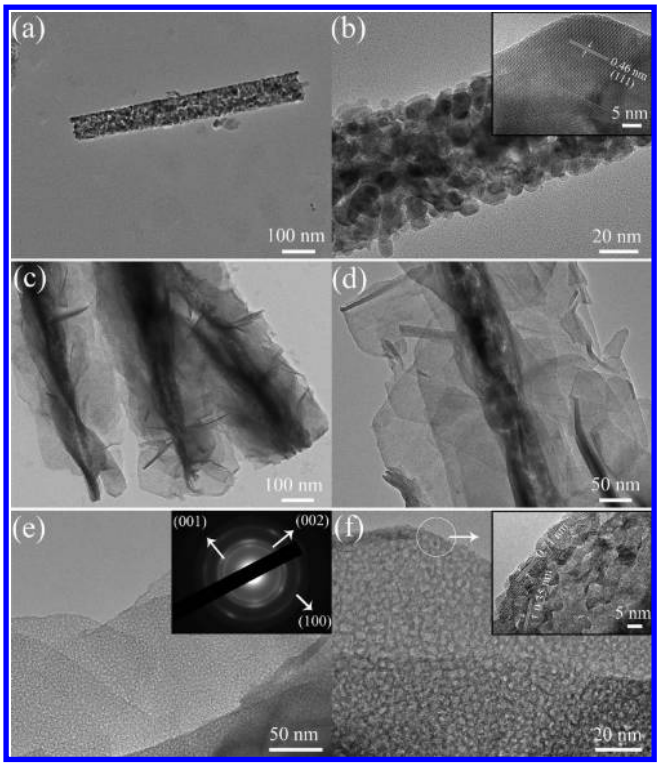

Figure 3. TEM characterization of the porous $Co(OH)_2$ nanosheet branches. (a, b) TEM images at different magnifications of the initial Co_3O_4 nanowires. Inset in (b) is the HRTEM atomic image of a single nanocrystallite. (c, d) $Co_3O_4/Co(OH)_2$ core/shell nanowire. (e, f) High-magnification TEM images of the $Co(OH)_2$ nanosheets. Inset in (e) is the corresponding SAED pattern and inset in (f) is the HRTEM image of the nanosheet.

good agreement with the (111) interplanar distance of the Co_3O_4 phase (JCPDS 42-1467). The core/shell nanowire architecture is clear as shown in Figure 3c,d. The Co_3O_4 core nanowire is tightly wrapped by the electrodeposited $Co(OH)_2$ nanosheets possessing numerous nanopits with diameters of ~3 nm. A polycrystalline SAED pattern of the nanosheet can be well indexed to the α-$Co(OH)_2$ phase (JCPDS 74-1057) (Figure 3e), and the lattice fringes with a lattice spacing of about 0.71 nm corresponds to the (001) planes of α-$Co(OH)_2$ (Figure 3f). Interestingly, the $Co_3O_4/Co(OH)_2$ core/shell nanowire arrays convert into homogeneous mesoporous Co_3O_4 core/shell nanowire arrays after annealing at 200 °C (Figure 4a,b). The $Co(OH)_2$ nanosheets decompose into mesoporous Co_3O_4 nanosheets with finer pores ranging from 2 to 5 nm (Figure 4c,d). This unique mesoporous morphological characteristic is favorable for electrolyte penetration and fast ion/electron transfer and may lead to enhanced electrochemical reactivity. Besides, the SAED pattern of the shell nanosheets confirms the existence of spinel polycrystalline Co_3O_4, and the lattice fringes with lattice spacing of 0.46 and 0.24 nm correspond to the (111) and (311) planes of Co_3O_4, respectively (Figure 4e). The phase change is also supported by the XRD result after heat treatment (Figure 4f). The typical

dx.doi.org/10.1021/cm302416d | Chem. Mater. 2012, 24, 3793−3799

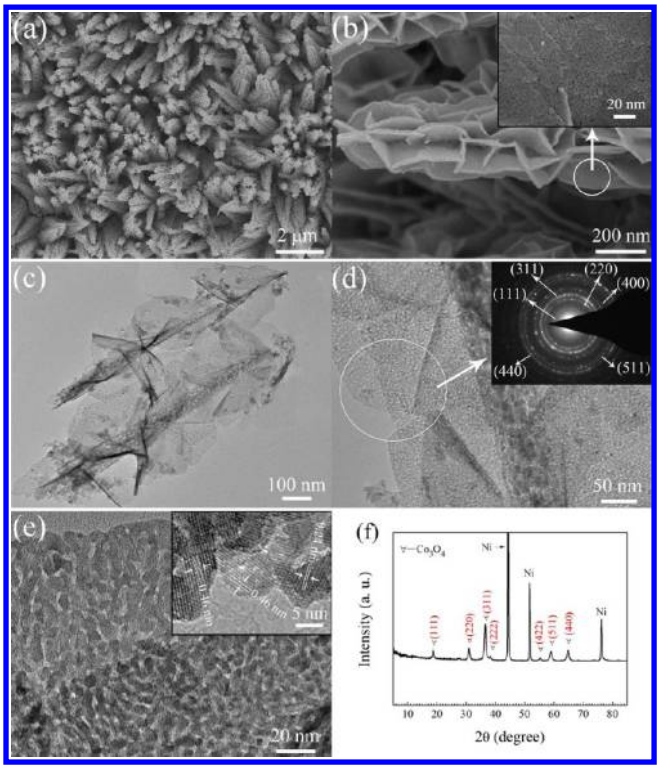

Figure 4. Conversion of $Co(OH)_2$ nanosheets to Co_3O_4 nanosheets and formation of homogeneous branched nanowire arrays. (a, b) SEM images of the Co_3O_4 core/shell nanowire arrays. (c) Low and (d) high magnification TEM images showing clearly the mesoporous core and nanosheets (SAED in inset). (e) HRTEM image of the mesoporous Co_3O_4 nanosheet. (f) XRD pattern (Ni signal is from the nickel foam substrate).

diffraction peaks of α-$Co(OH)_2$ disappear, and only peaks of Co_3O_4 are noticed.

In our experiment, the composition and thickness of the shell branches materials can be easily varied by choosing different reagents and deposition times due to the flexibility of the electrodeposition methods. We also prepared Co_3O_4/$Mn(OH)_2$ core/shell nanowire arrays via the same methodology (Supporting Information Figure S3). The $Mn(OH)_2$ nanosheet branches can be electrochemically assembled on the Co_3O_4 core nanowires to form core/shell nanowire arrays, which change into porous Co_3O_4/Mn_3O_4 core/shell nanowire arrays after annealing at 300 °C (Supporting Information Figure S4).

The growth mechanisms of Co_3O_4 nanowire array and metal hydroxide nanosheets are proposed as below. The freestanding Co_3O_4 nanowire array comes from basic cobalt carbonate hydroxide $Co_2(OH)_2CO_3$ nanowire arrays after heat-treatment. The reactions involved may be illustrated as follows.[20−22]

$$Co^{2+} + xF^- \rightarrow [CoF_x]^{(x-2)-} \quad (1)$$

$$H_2NCONH_2 + H_2O \rightarrow 2NH_3 + CO_2 \quad (2)$$

$$CO_2 + H_2O \rightarrow CO_3^{2-} + 2H^+ \quad (3)$$

$$NH_3{\cdot}H_2O \rightarrow NH_4^+ + OH^- \quad (4)$$

$$[CoF_x]^{(x-2)-} + 0.5(2-y)CO_3^{2-} + yOH^- + nH_2O \rightarrow Co(OH)_y(CO_3)_{0.5(2-y)}{\cdot}nH_2O + xF^- \quad (5)$$

$$3Co(OH)_y(CO_3)_{0.5(2-y)}{\cdot}nH_2O + \frac{1}{2}O_2 \xrightarrow{\text{Annealing}} Co_3O_4 + (3n + 1.5y)H_2O + 1.5(2-y)CO_2 \quad (6)$$

The Co_3O_4 nanowire consists of numerous interconnected nanocrystallites and possesses a large quantity of mesopores, which is ascribed to the successive release and loss of CO_2 and H_2O during the thermal decomposition of $Co_2(OH)_2CO_3$ precursor. For the electrodeposition of metal (Co or Mn) hydroxides on Co_3O_4 nanowires, the electrodeposition processes include an electrochemical reaction and a precipitation reaction, as expressed as follows.[23]

$$NO_3^- + H_2O + 2e^- \rightarrow NO_2^- + 2OH^- \quad (7)$$

$$M^{2+} + 2OH^- \rightarrow M(OH)_2 \quad (M = Co, Mn) \quad (8)$$

The preferential nanoflake growth of $Co(OH)_2$ and $Mn(OH)_2$ is a result of their layered brucite crystal structure of the CdI_2 type, which has a weak interaction between layers and strong binding within the layered planes. Neighboring layers are bound together by weak van der Waal forces, and thus the (001) planes are stable ones with the lowest surface energy. Taken together, the presented synthesis method is very robust and may lead to growth of other oxide/hydroxide and oxide/oxide core/shell nanowire arrays on various conductive substrates. These core/shell nanowire arrays show some interesting characteristics such as high porosity and direct growth on conductive substrates, which make them potential building blocks for electrochemical energy storage and catalysis.

As a preliminary study, we investigated the electrochemical properties of the Co_3O_4/$Co(OH)_2$ and mesoporous Co_3O_4 core/shell nanowire arrays grown on nickel foam for pseudocapacitor and lithium ion batteries applications, respectively. The pseudocapacitive properties of the Co_3O_4/$Co(OH)_2$ core/shell nanowire arrays are investigated by cyclic voltammograms and galvanostatic charge/discharge tests. Figure 5a shows the cyclic voltammogram (CV) curve of the Co_3O_4/$Co(OH)_2$ core/shell nanowire arrays at a scan rate of 10 mV s^{-1}. Two pairs of redox peaks (A1/C1 and A2/C2) are noticed in the CV curve, which correspond to the redox couples of $Co(OH)_2$/CoOOH and Co_3O_4/CoOOH, respectively.[5,24−27] Though $Co(OH)_2$ and Co_3O_4 will both convert into CoOOH, their intrinsic reaction potentials are different leading to two distinct redox couples. Discharge profiles of the Co_3O_4/$Co(OH)_2$ core/shell nanowire arrays at various discharge current densities and corresponding specific capacitances are shown in Figure 5b,c. The specific capacitances are calculated by subtracting the discharge time of bare nickel foam at the same current density, respectively. The detailed supercapacitor performances of the mesoporous Co_3O_4 nanowire arrays and nickel foam substrates have been discussed in our previous paper.[13] The Co_3O_4/$Co(OH)_2$ core/shell nanowire arrays show specific capacitances of 1095 F/g (1 A/g), 1034 F/g (2 A/g), 980 F/g (4 A/g), 916 F/g (10 A/g), 880 F/g (20 A/g), and 812 F/g (40 A/g). These values are much higher than those of the single Co_3O_4 nanowire arrays (323 F/g at 40 A/g and 248 F/g at 40 A/g) and other metal oxides films such as NiO and MnO_2.[28−30] Besides, the Co_3O_4/$Co(OH)_2$ core/shell nanowire arrays exhibit good cycling stability. The cycle characteristic of the core/shell arrays at 2 A/g is presented in Figure 5d. After 2000 cycles, the Co_3O_4/$Co(OH)_2$ core/shell nanowire arrays present a capacitance of 915 F/g with

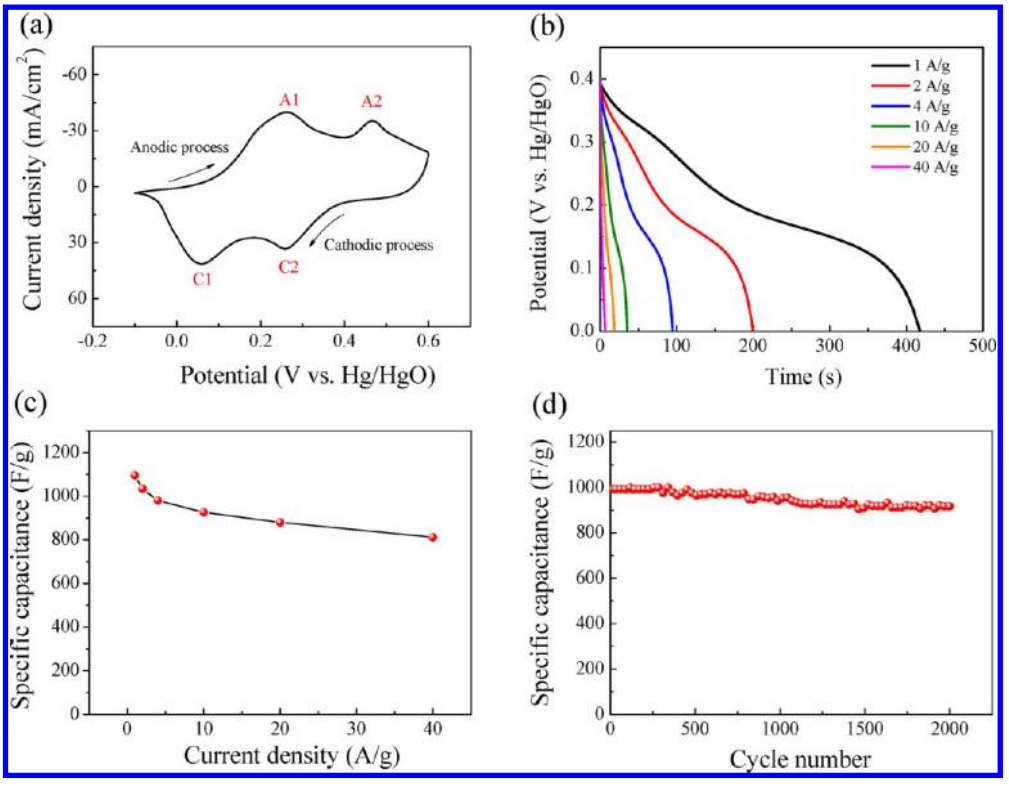

Figure 5. $Co_3O_4/Co(OH)_2$ core/shell nanowire arrays on nickel foam as the supercapacitor cathode. (a) CV curves at the scanning rate of 10 mV/s at the second cycle. (b) Discharge curves and (c) corresponding specific capacitances at various discharge current densities. (d) Cycling performance at 2 A/g.

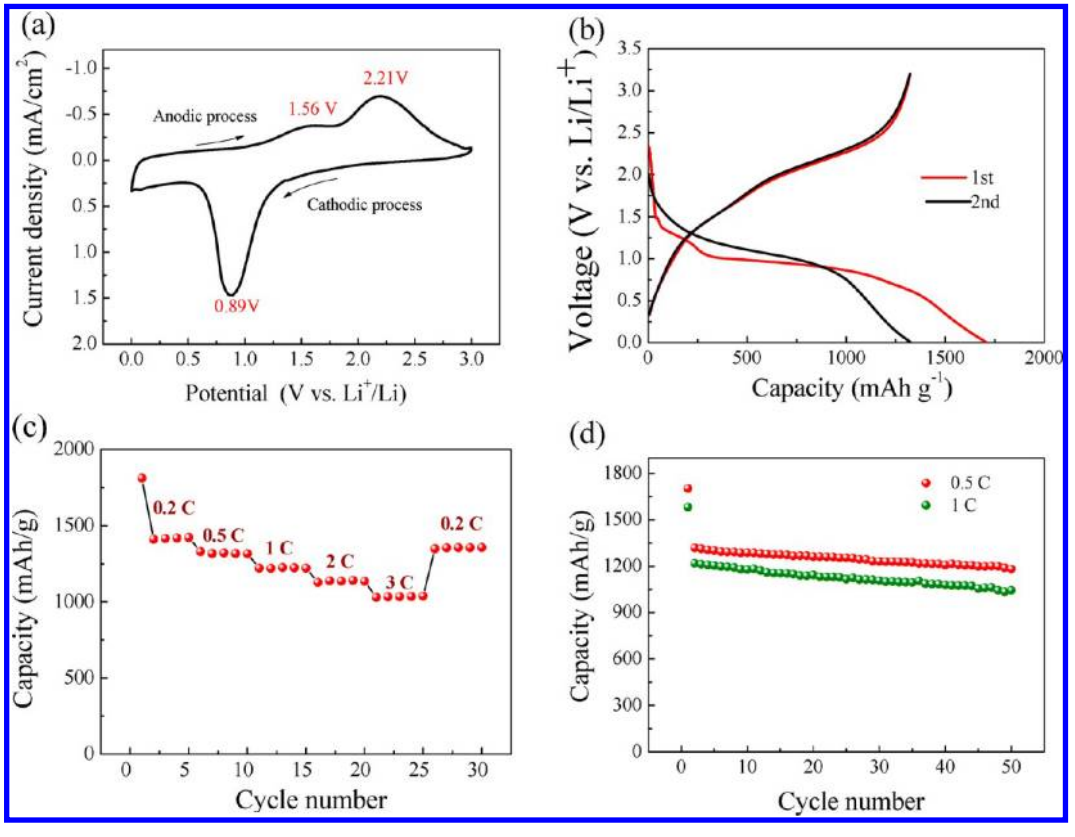

Figure 6. Mesoporous Co_3O_4 homogeneous core/shell nanowire arrays on nickel foam as the Li-ion battery anode. (a) CV curve at a scanning rate of 0.1 mV/s at the second cycle; (b) the discharge/charge curves; (c) rate capability and (d) cycling performance at different rates.

dx.doi.org/10.1021/cm302416d | *Chem. Mater.* 2012, 24, 3793−3799

92% of the maximum value, much better that the single $Co(OH)_2$ flakes grown on nickel foam (648 F/g with 73.6%)[24] and stainless steel (375 F/g with 68%).[31] Moreover, the core/shell nanowire array architecture is well maintained after 2000 cycles (Supporting Information Figure S5), indicating this core/shell architecture has a good mechanical stability. The enhanced pseudocapacitive performances are mainly due to the following two factors: (i) Both Co_3O_4 and $Co(OH)_2$ are active pseudocapacitive materials and show different reductive reaction potentials, which extend the discharge plateau contributing to more electrochemical energy storage.[32,33] (ii) The porous core/shell array configuration enables the fully exposure of both active materials to the electrolyte and provides a short diffusion path for both electrons and ions, thus leading to faster kinetics and higher utilization of active material.

As another demonstration, the homogeneous mesoporous Co_3O_4 core/shell nanowire arrays obtained by thermal conversion of the above $Co_3O_4/Co(OH)_2$ sample were applied as the anode material for lithium ion batteries. To understand the electrochemical process in detail, the CV curve is recorded first (Figure 6a). The reduction peak at 0.89 V corresponds to reduction of Co_3O_4 to metallic Co. During the following anodic process, the oxidation peak at 1.56 V is associated with the partial decomposition of the solid electrolyte interphase (SEI) layer, and another oxidation peak at 2.21 V corresponds to the decomposition of Li_2O leading to the formation of Co_3O_4.[34,35] It is well accepted that the electrochemical reaction mechanism between transition metal oxides with Li is different from the classical mechanisms based either on reversible insertion/deinsertion of lithium into host structures or on lithium alloying reactions. The electrochemical reactions between Co_3O_4 and Li can be expressed as follows.[36]

$$Co_3O_4 + 8Li^+ + 8e^- \leftrightarrow 4Li_2O + 3Co \quad \text{(cathode)} \tag{9}$$

$$8Li \leftrightarrow 8Li^+ + 8e^- \quad \text{(anode)} \tag{10}$$

$$Co_3O_4 + 8Li^+ \leftrightarrow 4Li_2O + 3Co \quad \text{(Overall)} \tag{11}$$

Figure 6b shows the discharge/charge curves of the Co_3O_4 core/shell nanowire arrays measured between 0.02 and 3.0 V versus Li/Li^+ at 0.5 C rate (1C = 890 mA/g). For the first discharge process, the discharge plateau is at ~0.9 V due to the conversion from Co_3O_4 to Co, which is consistent with the CV result. The discharge plateau becomes higher at the second cycle. The porous Co_3O_4 core/shell nanowire arrays show a first discharge capacity of 1703 mAh/g, much higher than the theoretical value (890 mAh/g). The extra capacity is attributed to the formation of solid electrolyte interphase (SEI) at the first discharge process.[36,37] This SEI layer is a gel-like film with complex components containg ethylene oxide based oligomers, LiF, Li_2CO_3, and lithium alkyl carbonate ($ROCO_2Li$). Tarascon and co-workers have observed the formation of SEI layer by ex situ TEM at the potential range of 1 to 0.02 V.[38] This phenomenon happens in other 3d transition metal oxides such as NiO, CoO, CuO, and Fe_3O_4.[16,36,39−42] The irreversible capacity loss between the first discharge and charge is attributed to the incomplete decomposition of both the SEI and Li_2O. The initial Coulombic efficiency of the Co_3O_4 core/shell nanowire arrays is calculated to be ~77.7%, higher than that of the Co_3O_4 power electrode (65%),[34] and comparable to other highly porous Co_3O_4 array films.[43] Impressively, the mesoporous Co_3O_4 core/shell nanowire arrays present superior rate capability and cycling stability (Figure 6c). The mesoporous Co_3O_4 core/shell nanowire arrays deliver a capacity of 1410 mAh/g at 0.2 C, 1323 mAh/g at 0.5 C, 1221 mAh/g at 1 C, 1136 mAh/g at 2 C, and 1033 mAh/g at 3C, respectively. Additionally, the specific capacities after 50 cycles at 0.5 C and 1 C rates are 1182, mAh g^{-1} and 1044 mAh/g, respectively, demonstrating the capability for a high cycling rate. Note the fact that the mesoporous Co_3O_4 core/shell nanowire arrays still show high discharge values over the theoretical capacity after cycling. A similar phenomenon has been reported by other authors. For example, Nam et al.[35] reported a reversible capacity of ~1200 mAh/g of Co_3O_4 nanowire arrays prepared via virus template. Du et al.[34] also demonstrated the high capacity over 1200 mAh/g of the Co_3O_4 nanotube. The reason for these high values is still unclear, but it is implied that the excess capacity is due to contribution from the partial decomposition of SEI films.

The high capacity and cycling stability of the homogneous Co_3O_4 nanobranches as anode for lithium ion battery are believed to benefit from the porous core/shell nanoarray configuration. (1) The highly porous system shortens the transportation/diffusion path for both electrons and Li ions, thus resulting in faster kinetics and high-rate capability; (2) high surface area (Supporting Information Figure S6) of the mesoporous nanowire arrays favors the efficient contact between active materials and electrolytes, providing more active sites for electrochemical reactions; and (3) the porous core/shell nanowire array architecture possesses favorable morphological stability, which helps to alleviate the structure damage caused by volume expansion during the cycling process. The porous Co_3O_4 core/shell nanowire arrays maintain the initial morphology after the lithiation/delithiation cycles (Supporting Information Figure S7). In short, these characteristics would lead to fast ion/electron transfer, sufficient contact between active materials and electrolyte, and enhanced flexibility, finally resulting in enhanced electrochemical performance.

■ CONCLUSIONS

We have demonstrated the fast and convenient method for the growth of porous oxides/hydroxides by direct electrodeposition on preformed nanowires toward the formation of hierarchical core/shell nanowire arrays. Examples include $Co_3O_4/Co(OH)_2$ and $Co_3O_4/Mn(OH)_2$) core/shell nanowire arrays on different conductive substrates. The hydroxide shell has a highly porous structure with numerous meso- and macropores, and when converted to oxides by thermal annealing, the porous structure is preserved. For their application in energy storage, the $Co_3O_4/Co(OH)_2$ and mesoporous Co_3O_4 core/shell nanowire arrays display outstanding electrochemical performances in supercapacitor and lithium ion batteries, respectively. This fabrication method can be readily applied to arbitrary substrates including metal nanowire network, inverse opals, and 3D graphene, providing a wide range of possibilities for different applications of these porous metal oxides/hybrids.

■ ASSOCIATED CONTENT

Ⓢ Supporting Information

SEM images of Co_3O_4 nanowire arrays and corresponding XRD pattern; SEM images of $Co_3O_4/Co(OH)_2$ core/shell nanowire arrays on stainless steel and Ti foil substrates; SEM and TEM images of $Co_3O_4/Mn(OH)_2$ core/shell nanowire arrays and corresponding XRD pattern and the converted Co_3O_4/Mn_3O_4 nanowire arrays; SEM images of the $Co_3O_4/$

$Co(OH)_2$ core/shell nanowire arrays after cycling for 2000 cycles at 2 A/g; BET measurement of mesoporous Co_3O_4 core/shell nanowire arrays; and SEM image of the mesoporous Co_3O_4 core/shell nanowires after 10 LIB cycles at 0.5 C. This material is available free of charge via the Internet at http://pubs.acs.org.

AUTHOR INFORMATION

Corresponding Author

*E-mail: fanhj@ntu.edu.sg (H.J.F), tujp@zju.edu.cn (J.P.T).

Notes

The authors declare no competing financial interest.

ACKNOWLEDGMENTS

The authors would like to acknowledge financial support from Fundamental Research Funds for the Central Universities (2011QNA4006), Opening Foundation of Zhejiang Provincial Top Key Discipline (20110936) and Key Science and Technology Innovation Team of Zhejiang Province (2010R50013).

REFERENCES

(1) Law, M.; Goldberger, J.; Yang, P. D. *Annu. Rev. Mater. Res.* **2004**, *34*, 83−122.
(2) van Embden, J.; Jasieniak, J.; Gomez, D. E.; Mulvaney, P.; Giersig, M. *Aust. J. Chem.* **2007**, *60* (7), 457−471.
(3) Ding, L.-X.; Li, G.-R.; Wang, Z.-L.; Liu, Z.-Q.; Liu, H.; Tong, Y.-X. *Chem.−Eur. J.* **2012**, *18* (27), 8386−8391.
(4) Li, L.; Yang, Y. W.; Li, G. H.; Zhang, L. D. *Small* **2006**, *2* (4), 548−553.
(5) Liu, J. P.; Jiang, J.; Cheng, C. W.; Li, H. X.; Zhang, J. X.; Gong, H.; Fan, H. J. *Adv. Mater.* **2011**, *23* (18), 2076.
(6) Wang, K.; Chen, J.; Zhou, W.; Zhang, Y.; Yan, Y.; Pern, J.; Mascarenhas, A. *Adv. Mater.* **2008**, *20* (17), 3248−3253.
(7) Agarwal, R. *Small* **2008**, *4* (11), 1872−1893.
(8) Liu, R.; Lee, S. B. *J. Am. Chem. Soc.* **2008**, *130* (10), 2942−2943.
(9) Chen, J.; Xia, X. H.; Tu, J. P.; Xiong, Q. Q.; Yu, Y. X.; Wang, X. L.; Gu, C. D. *J. Mater. Chem.* **2012**, *22* (30), 15056−15061.
(10) Chueh, Y. L.; Hsieh, C. H.; Chang, M. T.; Chou, L. J.; Lao, C. S.; Song, J. H.; Gan, J. Y.; Wang, Z. L. *Adv. Mater.* **2007**, *19* (1), 143.
(11) Li, G. R.; Wang, Z. L.; Zheng, F. L.; Ou, Y. N.; Tong, Y. X. *J. Mater. Chem.* **2011**, *21* (12), 4217−4221.
(12) He, Y. B.; Li, G. R.; Wang, Z. L.; Su, C. Y.; Tong, Y. X. *Energy Environ. Sci.* **2011**, *4* (4), 1288−1292.
(13) Xia, X.; Tu, J.; Zhang, Y.; Wang, X.; Gu, C.; Zhao, X.-b.; Fan, H. J. *ACS Nano* **2012**, *6* (6), 5531−5538.
(14) Zhao, X. H.; Wang, P.; Li, B. J. *Chem. Commun.* **2010**, *46* (36), 6768−6770.
(15) Marcu, A.; Yanagida, T.; Nagashima, K.; Oka, K.; Tanaka, H.; Kawai, T. *Appl. Phys. Lett.* **2008**, *92*, 173119.
(16) Liu, C.; Li, F.; Ma, L. P.; Cheng, H. M. *Adv. Mater.* **2010**, *22* (8), E28.
(17) Li, Y. G.; Tan, B.; Wu, Y. Y. *J. Am. Chem. Soc.* **2006**, *128* (44), 14258−14259.
(18) Guan, C.; Liu, J. P.; Cheng, C. W.; Li, H. X.; Li, X. L.; Zhou, W. W.; Zhang, H.; Fan, H. J. *Energy Environ. Sci.* **2011**, *4* (11), 4496−4499.
(19) Liu, J. P.; Cheng, C. W.; Zhou, W. W.; Li, H. X.; Fan, H. J. *Chem. Commun.* **2011**, *47* (12), 3436−3438.
(20) Jiang, J.; Liu, J. P.; Huang, X. T.; Li, Y. Y.; Ding, R. M.; Ji, X. X.; Hu, Y. Y.; Chi, Q. B.; Zhu, Z. H. *Cryst. Growth Des.* **2010**, *10* (1), 70−75.
(21) Xia, X. H.; Tu, J. P.; Zhang, Y. Q.; Mai, Y. J.; Wang, X. L.; Gu, C. D.; Zhao, X. B. *RSC Adv.* **2012**, *2* (5), 1835−1841.
(22) Xu, R.; Zeng, H. C. *J. Phys. Chem. B* **2003**, *107* (46), 12643−12649.
(23) Xia, X. H.; Tu, J. P.; Xiang, J. Y.; Huang, X. H.; Wang, X. L.; Zhao, X. B. *J. Power Sources* **2010**, *195* (7), 2014−2022.
(24) Xia, X. H.; Tu, J. P.; Zhang, Y. Q.; Mai, Y. J.; Wang, X. L.; Gu, C. D.; Zhao, X. B. *J. Phys. Chem. C* **2011**, *115* (45), 22662−22668.
(25) Zhou, W. J.; Zhang, J.; Xue, T.; Zhao, D. D.; Li, H. L. *J. Mater. Chem.* **2008**, *18* (8), 905−910.
(26) Gao, Y. Y.; Chen, S. L.; Cao, D. X.; Wang, G. L.; Yin, J. L. *J. Power Sources* **2010**, *195* (6), 1757−1760.
(27) Meher, S. K.; Rao, G. R. *J. Phys. Chem. C* **2011**, *115* (31), 15646−15654.
(28) Xia, X. H.; Tu, J. P.; Wang, X. L.; Gu, C. D.; Zhao, X. B. *J. Mater. Chem.* **2011**, *21* (3), 671−679.
(29) Xue, T.; Xu, C. L.; Zhao, D. D.; Li, X. H.; Li, H. L. *J. Power Sources* **2007**, *164* (2), 953−958.
(30) Chou, S. L.; Wang, J. Z.; Chew, S. Y.; Liu, H. K.; Dou, S. X. *Electrochem. Commun.* **2008**, *10* (11), 1724−1727.
(31) Chou, S. L.; Wang, J. Z.; Liu, H. K.; Dou, S. X. *J. Electrochem. Soc.* **2008**, *155* (12), A926−A929.
(32) Xia, X. H.; Tu, J. P.; Mai, Y. J.; Wang, X. L.; Gu, C. D.; Zhao, X. B. *J. Mater. Chem.* **2011**, *21* (25), 9319−9325.
(33) Rakhi, R. B.; Chen, W.; Cha, D. Y.; Alshareef, H. N. *Nano Lett.* **2012**, *12* (5), 2559−2567.
(34) Du, N.; Zhang, H.; Chen, B.; Wu, J. B.; Ma, X. Y.; Liu, Z. H.; Zhang, Y. Q.; Yang, D.; Huang, X. H.; Tu, J. P. *Adv. Mater.* **2007**, *19* (24), 4505.
(35) Nam, K. T.; Kim, D. W.; Yoo, P. J.; Chiang, C. Y.; Meethong, N.; Hammond, P. T.; Chiang, Y. M.; Belcher, A. M. *Science* **2006**, *312* (5775), 885−888.
(36) Cheng, F.; Tao, Z.; Liang, J.; Chen, J. *Chem. Mater.* **2008**, *20* (3), 667−681.
(37) Tarascon, J. M.; Armand, M. *Nature* **2001**, *414* (6861), 359−367.
(38) Grugeon, S.; Laruelle, S.; Herrera-Urbina, R.; Dupont, L.; Poizot, P.; Tarascon, J. M. *J. Electrochem. Soc.* **2001**, *148* (4), A285−A292.
(39) Poizot, P.; Laruelle, S.; Grugeon, S.; Dupont, L.; Tarascon, J. M. *Nature* **2000**, *407* (6803), 496−499.
(40) Xiong, Q. Q.; Tu, J. P.; Lu, Y.; Chen, J.; Yu, Y. X.; Qiao, Y. Q.; Wang, X. L.; Gu, C. D. *J. Phys. Chem. C* **2012**, *116* (10), 6495−6502.
(41) Mai, Y. J.; Shi, S. J.; Zhang, D.; Lu, Y.; Gu, C. D.; Tu, J. P. *J. Power Sources* **2012**, *204*, 155−161.
(42) Xiang, J. Y.; Tu, J. P.; Zhang, L.; Zhou, Y.; Wang, X. L.; Shi, S. J. *J. Power Sources* **2010**, *195* (1), 313−319.
(43) Li, Y. G.; Tan, B.; Wu, Y. Y. *Nano Lett.* **2008**, *8* (1), 265−270.